

Article

Research on Shock Acceleration Limit of an Ultra-Stable Optical Cavity for Space Applications Based on the Finite Element Methodology

Guanjun Xu ^{1,2,†}, Dongdong Jiao ^{2,†}, Long Chen ², Linbo Zhang ², Jun Liu ², Ruifang Dong ^{2,*}, Tao Liu ² and Junbiao Wang ¹

¹ School of Mechanical Engineering, Northwestern Polytechnical University, Xi'an 710072, China; xuguanjun@ntsc.ac.cn (G.X.); wangjunb@nwpu.edu.cn (J.W.)

² National Time Service Center, Chinese Academy of Sciences, Xi'an 710600, China; jiaodd@ntsc.ac.cn (D.J.); chenlong@ntsc.ac.cn (L.C.); linbo@ntsc.ac.cn (L.Z.); liujun@ntsc.ac.cn (J.L.); taoliu@ntsc.ac.cn (T.L.)

* Correspondence: dongruifang@ntsc.ac.cn

† These authors contributed equally to this work.



Citation: Xu, G.; Jiao, D.; Chen, L.; Zhang, L.; Liu, J.; Dong, R.; Liu, T.; Wang, J. Research on Shock Acceleration Limit of an Ultra-Stable Optical Cavity for Space Applications Based on the Finite Element Methodology. *Crystals* **2021**, *11*, 998. <https://doi.org/10.3390/cryst11080998>

Academic Editors: Jingsong Li, Qingli Zhang, Zhirong Zhang and Shujun Zhang

Received: 30 July 2021

Accepted: 20 August 2021

Published: 22 August 2021

Publisher's Note: MDPI stays neutral with regard to jurisdictional claims in published maps and institutional affiliations.



Copyright: © 2021 by the authors. Licensee MDPI, Basel, Switzerland. This article is an open access article distributed under the terms and conditions of the Creative Commons Attribution (CC BY) license (<https://creativecommons.org/licenses/by/4.0/>).

Abstract: Ultra-stable optical cavities (USOCs) as fragile precision instruments have many important applications in space. In order to protect them from being damaged during a rocket launch, we analyzed a USOC by means of finite element methodology. The shock acceleration limits that the USOC can withstand in different directions and under various conditions are given. To increase the shock acceleration limit, the midplane thickness and the fixed hole diameter should be selected to be as high as possible. It is worth noting that the launch direction of the USOC should be selected as the horizontal direction, for which the shock acceleration limit that the USOC can withstand is approximately two times that of the vertical direction. In this paper, results provide guidance for the design of USOCs for space applications, especially the design to prevent the damage caused by a shock. The method could then be applied to other space optical cavities, providing a tool to improve the effect of shock at high accelerations.

Keywords: ultra-stable laser; ultra-stable optical cavity; shock acceleration; space applications; finite element analysis

1. Introduction

Ultra-stable lasers are key elements in many domains, including frequency metrology [1–5], gravitational wave detection [6], fundamental physics tests [7,8], and coherent optical links [9,10]. Ultra-stable lasers can be produced by locking lasers onto USOCs with the Pound–Drever–Hall (PDH) technique, and the instability of an ultra-stable laser frequency can be defined with the stability of the optical length of a USOC [11–14], which is generally machined with ultra-low-expansion glass (ULE). However, most ultra-stable lasers have been constrained to operate in well-controlled laboratory environments. There is growing interest in frequency-stable lasers capable of operating outside a laboratory for applications such as space optical clocks, geodesy, tests of fundamental physics in space, and the generation of ultra-stable microwaves for radar [15–18]. Hence, it is important to investigate transportable USOCs to determine whether an ultra-stable laser can operate in a non-laboratory environment [17–19].

To this end, different groups have designed a variety of shapes and support modes for USOCs [15–36]. In 2011, Leibrandt et al. designed a spherical USOC that was rigidly supported at two points on a diameter with a squeeze-insensitive angle [15,16,20]. Acceleration sensitivities below 3×10^{-10} /g were achieved. In the same year, Webster et al. constructed a cubic USOC with four supports placed in a tetrahedral configuration [18]. An acceleration sensitivity better than 2.5×10^{-11} /g was achieved. In 2012, Argence et al.

reported a cylinder USOC rigidly held at its mid-plane [19]. Acceleration sensitivities below $4 \times 10^{-10}/g$ were achieved. In 2014, Chen et al. constructed a cylinder USOC rigidly held at ten pairs of points on the cavity spacer [21] and acceleration sensitivities below $4 \times 10^{-10}/g$ were achieved. In 2018, a similar cuboid USOC was mounted rigidly and tested by dropping from a height of 25 cm, corresponding to an acceleration of 100 g [28]. In 2020, Chen et al. [31] designed and developed a cubic optical cavity with a side length of 100 mm based on the 50 mm cubic cavity designed by Webster et al. [18]. The vibration sensitivity of the three orthogonal directions was $10^{-10}/g$.

Compared with lab applications, USOCs with low vibration sensitivity used in the space face challenges, such as being rigidly held for transport, enduring larger vibration, and shock acceleration [15–22,27,28,31–36]. In the rocket launching stage, the shock acceleration loaded on a USOC can be hundreds of times greater than gravitational acceleration (9.8 m/s^2) [19,28,37,38]. Due to this, as a fragile precision instrument, the USOC may have unrecoverable structural failures and fractures [28,35,39–41]. To realize the space applications of the USOC, it must withstand the large shock of the rocket launching stage without damage. However, there is no in-depth study on this at present. In this paper, we focus on the effect of shock acceleration on USOCs for space applications, including Space Optical Clocks (SOCs) in Europe [18,19,25] and China [29]. It can provide design guidance for preventing damage caused by a shock in the space applications of USOCs.

The objective of this work was to protect the USOCs from being damaged by shock vibration during the rocket launching stage by giving the limit of shock acceleration. In this paper, we considered the cylindrical optical cavity rigidly mounted at its mid-plane designed by Argence et al. [19] and used finite element analysis (FEA) to study the effect of shock acceleration on the USOC for space applications. Firstly, the elastic deformation induced by the shock acceleration with frequency variation is simplified as the quasi-static elastic deformation based on the vibration dispersion relationship of the USOC. The failure criterion of the USOC, based on the maximum von Mises stress and the maximum tensile strength of the material was presented. Secondly, to calculate the maximum von Mises stress of the USOC induced by the shock acceleration, the FEA model of quasi-static mechanics was established. Thirdly, we calculated the maximum acceleration that the USOC could bear under different conditions, including the thickness T of the mid-plane (used for fixing the optical cavity), the diameter $\phi 1$ of the fixed hole, the shock acceleration directions, and the positions of the constraint.

The paper was organized as follows. In Section 2, the fundamental theories were presented, including the vibration dispersion relationship and failure criterion of the USOC. The FEA model of quasi-static mechanics is established in Section 3. The simulation results and the discussion are presented in Section 4. Finally, in Section 5, we present our discussions and conclusions.

2. Fundamental Principle

2.1. Quasi-Static Mechanics

The geometry model of the USOC (Ref. [19]) is described in Figure 1a, and the cylindrical USOC is rigidly mounted at its mid-plane by the fixed holes. The USOC can be simplified as a one-dimensional elastic molecular chain. Then, based on the vibration dispersion relationship of the solid materials, the vibration dispersion relationship of the USOC can be expressed by Equation (1) [14]:

$$\lambda = \sqrt{\frac{E}{\rho}} \frac{1}{f} \quad (1)$$

where E and ρ are the elastic modulus and the density of the USOC, respectively, while f and λ are the vibration frequency and the wavelength, respectively. For the ULE USOC, according to Equation (1) and Table 1, when the frequency is $f < 5000$ Hz, the wavelength is $\lambda > 1100$ mm (which is ten times the length of the USOC). In this work, the wavelength in the USOC is 100 mm, which is larger than the size of the cavity, and all the particles in

the USOC vibrate in the same phase, so the quasi-static mechanic analysis is sufficient to study its motion.

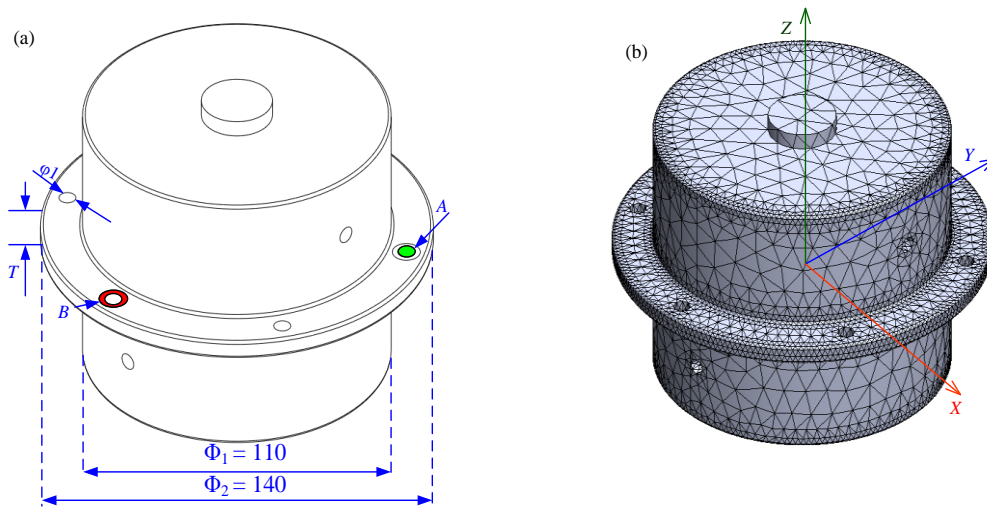


Figure 1. Geometrical and FEA models of the USOC (Ref. [19]). (a) The geometry model of the cavity: T is the thickness of the midplane of the USOC, and A and B represent two kinds of constraints in the FEA simulation. The diameter of the midplane is 140 mm. ϕ_1 represents the diameters of the holes used to fix the cavity. (b) The FEA model of the USOC meshed with tetrahedron elements.

Table 1. Material properties of ULE.

Parameters	Density (kg/m ³)	Young's Modulus (GPa)	Poisson's Ratio	Ultimate Tensile Stress (MPa)
Value	2210	67.6	0.17	49.8

2.2. Failure Criterion of the Ultra-Stable Optical Cavity

According to the widely used shape-change strength ratio theory (the fourth strength theory) in mechanical design [42], we checked the strength of the USOC, as shown in Figure 1. The failure criterion of the USOC can be expressed as Equation (2) [42]:

$$\frac{\sigma_{\max}}{K} \geq \sigma_{\text{von-Mises}} \quad (2)$$

where $\sigma_{\text{von-Mises}}$ is the maximum von Mises stress, σ_{\max} is the ultimate tensile stress of the material, and K is the safety coefficient. As a matter of convenience, $K = 1$ in this work. Based on Equation (2), when $\sigma_{\text{von-Mises}}$ is larger than σ_{\max} , the failure criterion of the USOC is met and it is thought to have fractured.

3. Model of the Finite Element Analysis

Figure 1a shows the USOC described in [19], that was mounted at its midplane with a mechanical interface and with a complex design involving vibration. The geometrical dimensions of the USOC are described (Figure 1a) in detail. The spacer was made of Ultra-Low Expansion (ULE) glass. To reduce the thermal noise, Fused Silica (FS) was used to make two mirror substrates with 25.4 mm diameters and 6.3 mm thicknesses.

In Table 1, the material properties of the ULE and FS are listed, including the elastic properties and the ultimate tensile stress of the structural failure. As described in Figure 1a, three out of six holes located at the midplane are used to fix the USOC, and these three holes are symmetrical at 120 degrees. In the FEA model, there are two kinds of positions of constraint (A and B), which are presented in Figure 1a. Constraint A : six degrees freedoms of the inner surface of the three holes are fully constrained. Constraint B : six degrees freedoms of the surface of the six pads for the three holes are fully constrained. As shown in Figure 2b, the USOC meshes have approximately 200,000 tetrahedral elements, for

which each tetrahedron has four nodes. In this work, it was assumed that there was only elastic deformation and no plastic deformation. The shock acceleration loaded on the USOC varied between 10 g (9.8 m/s^2) and 600 g (9.8 m/s^2). The directions of the shock acceleration included the vertical direction (Z-axis), horizontal direction (X-axis or Y-axis), and three orthogonal directions (X-axis, Y-axis, and Z-axis).

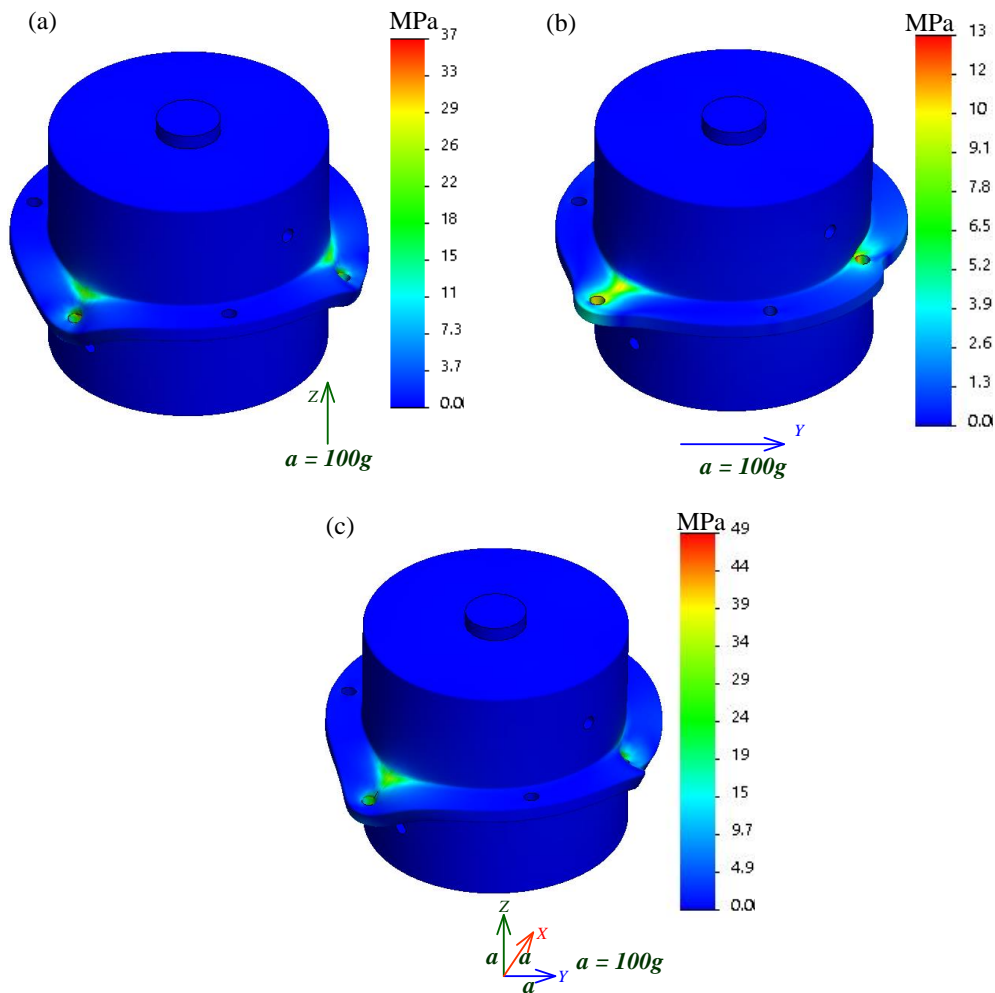


Figure 2. Deformation and von Mises stress of the USOC (Ref. [19]) loaded by the 100 g shock acceleration along different directions: (a) Vertical direction (Z-axis). (b) Horizontal direction (Y-axis). (c) Three orthogonal directions (X-axis, Y-axis, and Z-axis) (the deformation has been amplified by a factor of 5×10^3 for demonstration).

4. Results and Discussion

4.1. Deformation and Von Mises Stress Characteristics

The deformations and the von Mises stress of the USOC (Ref. [19]) are shown in Figure 2, which is loaded by a 100 g shock acceleration following by the three previously mentioned different directions. In general, the maximum von Mises stress is located at the three holes that fix the cavity and at the edge between the midplane and the spacer. The main reason for this may be that these locations are prone to stress concentration. The von Mises stresses that were located at the spacer and the two mirrors were approximately zero. Moreover, the deformation direction is almost the same as that of the shock acceleration. In that sense, and under the same conditions, it was determined that $\sigma_{\text{von-Mises}}$ along the vertical direction (Z-axis) was greater than that along the horizontal direction (Y-axis).

4.2. Effect of the Thickness T of the Mid-Plane on the Maximum von Mises Stress

Figure 3 shows the variation of $\sigma_{von-Mises}$ in the three directions of loading as a function of the shock acceleration and the thickness T of the mid-plane. Generally, for different thicknesses T of the midplane, a linear relationship will exist between $\sigma_{von-Mises}$ of the USOC and the shock acceleration with the different shock directions. As the thickness T of the mid-plane increases, $\sigma_{von-Mises}$ decreases. To protect the ULE USOC from being damaged during a rocket launch, the results show that the thickness T of the mid-plane should be the largest possible without affecting the performance of the USOC. The $\sigma_{von-Mises}$ loaded by the shock acceleration along the three orthogonal directions (X-axis, Y-axis, and Z-axis) was the largest, compared to the other two directions of loading. The main reason for this may be that the equivalent shock acceleration is the maximum under the same conditions. The $\sigma_{von-Mises}$ loaded by the shock along the vertical direction was three times that along the horizontal direction under the same conditions, therefore indicating that the launch direction of the USOC should be horizontal.

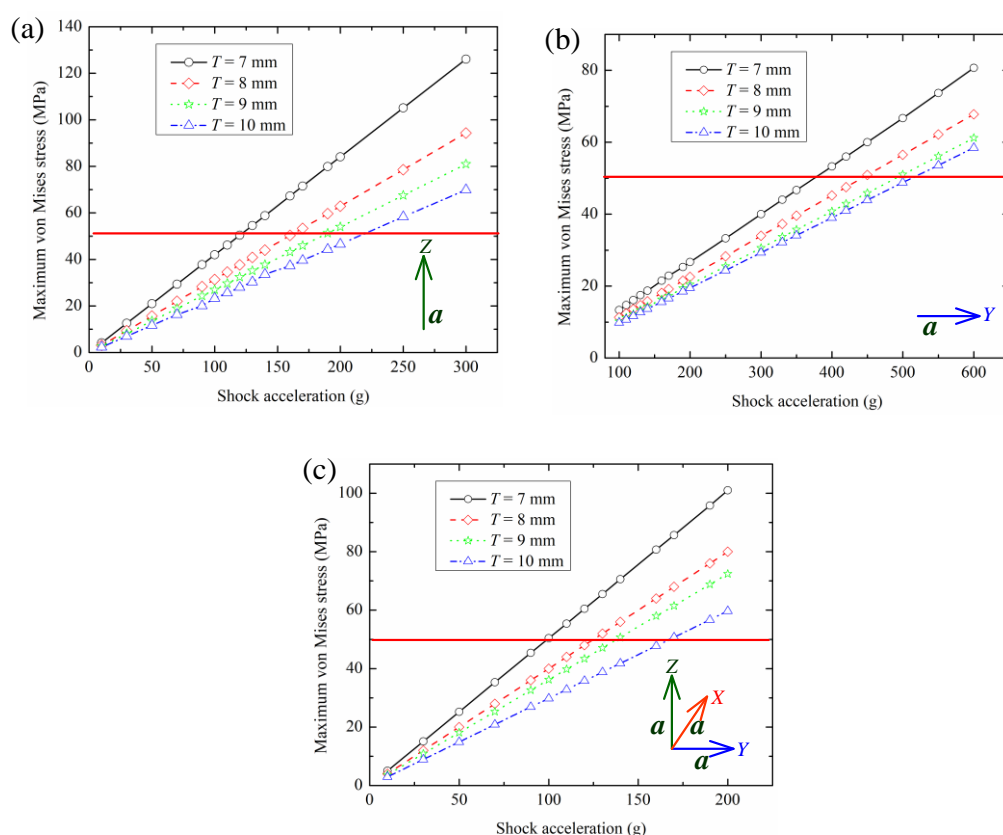


Figure 3. Variation of $\sigma_{von-Mises}$ as a function of the shock acceleration and the thickness T of the mid-plane as well as loading along the three directions: (a) Vertical direction (Z-axis). (b) Horizontal direction (Y-axis). (c) Three orthogonal directions (X-axis, Y-axis, and Z-axis). The black solid line with circles, red dashed line with squares, green dotted line with stars, and blue dash-dot line with triangles correspond to T equal 7 mm, 8 mm, 9 mm, and 10 mm, respectively. The red line represents the ultimate tensile stress σ_{max} of the material ULE of the USOC.

4.3. Effect of the Diameter $\phi 1$ of the Fixed Hole on the Maximum von Mises Stress

Figure 4 shows the variation of the $\sigma_{von-Mises}$ in the three directions of loading as a function of the shock acceleration as well as the diameter $\phi 1$ of the holes. Generally, the relationship between $\sigma_{von-Mises}$ and the shock acceleration with different shock directions with different $\phi 1$ is linear, similar to the relationship found when the T of the mid-plane was varied. The $\sigma_{von-Mises}$ with $\phi 1 = 4.1$ mm is larger than that with $\phi 1 = 6.1$ mm. To protect the ULE USOC from being fractured during a rocket launch with a large shock acceleration, the diameter $\phi 1 = 4.1$ mm of the holes should be as high as possible. The $\sigma_{von-Mises}$ loaded

by the shock acceleration along the three orthogonal directions (X-axis, Y-axis, and Z-axis) was also the largest, compared to the other two directions. We believe that the main reason for this is similar to that of the thickness T of the mid-plane. The $\sigma_{von-Mises}$ loaded by the shock along the horizontal direction is about one-third of that along the vertical direction under the same condition, which also indicates that the launch direction of the USOC should be horizontal.

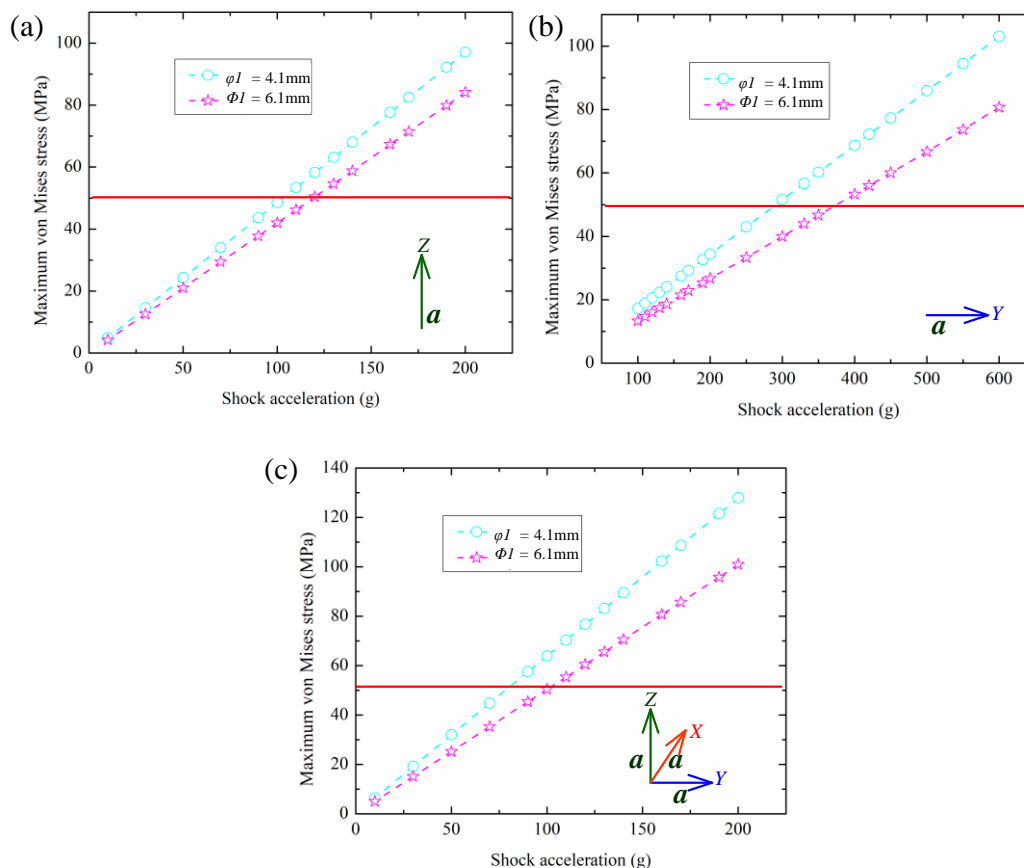


Figure 4. Variation of $\sigma_{von-Mises}$ as a function of the shock acceleration and the diameter ϕl of the holes used to fix the cavity (Figure 1) as well as a loading along the three directions: (a) Vertical direction (Z-axis). (b) Horizontal direction (Y-axis). (c) Three orthogonal directions (X-axis, Y-axis, and Z-axis). The cyan dashed line with circles and the magenta dashed line with stars represent $\sigma_{von-Mises}$ corresponding to diameters of 4.1 mm and 6.1 mm, respectively. The red line represents the ultimate tensile stress σ_{max} of the material ULE of the USOC.

4.4. Effect of the Positions of Constraint on the Maximum von Mises Stress

Two kinds of positional constraints were investigated, and the results of the $\sigma_{von-Mises}$ loaded with different directions are shown in Figure 5. Generally, for constraints A and B, there was also a linear relationship between $\sigma_{von-Mises}$ and the shock acceleration with different shock directions, and this relationship was similar to that of the thickness T of the mid-plane and the diameter ϕl . When the shock direction is vertical (Z-axis), $\sigma_{von-Mises}$ of constraint A is larger than that of constraint B. For the horizontal direction (Y-axis), the opposite is true. However, when the shock directions are along the three orthogonal directions (X-axis, Y-axis, and Z-axis), the gap between constraints A and B can be almost negligible. The $\sigma_{von-Mises}$ loaded by the shock accelerations along the three orthogonal directions (X-axis, Y-axis, and Z-axis) was also the largest, compared to the other two directions. The main reason for this was the similarity to the thickness T of the mid-plane and the diameter ϕl . For constraint A, $\sigma_{von-Mises}$ loaded by the shock along the horizontal direction was about one-third than along the vertical direction under the same conditions. However, for constraint A, the $\sigma_{von-Mises}$ loaded by the shock along the horizontal direction

was almost equal to that along the vertical direction under the same conditions. Overall, this also indicates that the launch direction of the USOC should be horizontal.

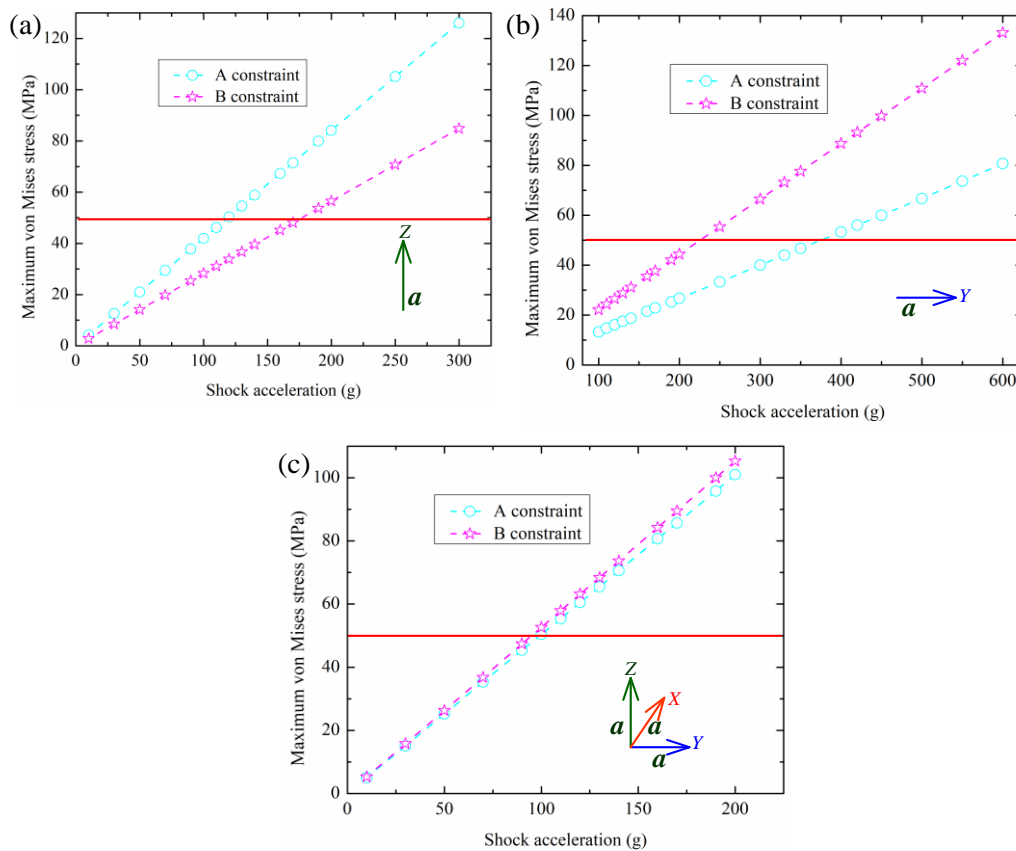


Figure 5. Variation of $\sigma_{von-Mises}$ as a function of the shock acceleration and the constraint position of the holes used to fix the cavity as well as the loading along the three directions: (a) Vertical direction (Z-axis). (b) Horizontal direction (Y-axis). (c) Three orthogonal directions (X-axis, Y-axis, and Z-axis). (Figure 1). The cyan dashed line with circles and the magenta dashed line with stars represent $\sigma_{von-Mises}$ corresponding to constraints A and B, respectively. The red line represents the ultimate tensile stress σ_{max} of the material ULE of the USOC.

4.5. Shock Acceleration Limit

The maximum shock acceleration that the USOC could withstand is presented in Table 2, where the safety factor is defined as $K = 1$. Generally, the maximum shock acceleration along the horizontal direction (X-axis or Y-axis) that the USOC can withstand is about two times that of the vertical direction (Z-axis) and three times that of the three orthogonal directions (X-axis, Y-axis, and Z-axis). As the thickness T of the mid-plane and the diameters of the holes increase, the maximum shock accelerations also increase. When $T = 10$ mm, $\varphi1 = 6.1$ mm, and $K = 1$, the maximum shock acceleration that the optical cavity can withstand is 508 g along the horizontal direction. In summary, for a USOC designed for space applications, based on the results of this work, the optimal launch direction should be the horizontal direction, and the values of T and $\varphi1$ should be selected to be as high as possible.

Table 2. Maximum shock acceleration that the ultra-stable optical cavity can withstand.

Shock Direction	T (mm)				$\phi 1$ (mm)		Constraint	
	7	8	9	10	4.1	6.1	A	B
Vertical (g)	119	158	185	220	102	119	119	178
Horizontal (g)	374	440	488	508	290	374	374	224
Three orthogonal (g)	99	125	138	167	78	99	99	94

5. Discussions and Conclusions

USOCs as fragile precision instruments are important elements in many domains of space applications. To protect the USOCs from being damaged by shock vibration during the rocket launching stage, this research investigates the effect of the shock on a USOC for space applications in detail through FEA. Compared with previous studies, we give the shock acceleration limit that the USOC can withstand and methods to improve the shock resistance for the first time.

The maximum von Mises stresses of the optical cavity under different conditions were studied, including the thickness T of the mid-plane, the constraint positions, the shock acceleration directions, and the diameter $\phi 1$ of the holes. Results show that there is a linear relationship between $\sigma_{von-Mises}$ and the shock acceleration along different directions. As the thickness T and the diameter $\phi 1$ increase, $\sigma_{von-Mises}$ decreases. The different constraint positions affect $\sigma_{von-Mises}$ along the vertical direction and the horizontal direction. However, the gap for the three orthogonal directions can be ignored. Results of FEA simulations also showed that the optimal rocket launch direction of the USOC is horizontal, for which the maximum shock acceleration that the USOC can withstand is about two times that of a launch along the vertical direction and three times that of a launch along the three orthogonal directions.

When $T = 10$ mm, $\phi 1 = 6.1$ mm, and $K = 1$, the maximum shock acceleration that the optical cavity can withstand is about 508 g along the horizontal direction. To protect the USOC in the rocket launch stage, the thickness T and the diameter $\phi 1$ should be selected to be as high as possible. Noting that the results of our research show that changing the launch direction is also one of the effective methods to improve the shock resistance, which has not been reported in previous studies. Our method can be readily extended to other space optical cavities, thus providing a powerful tool for improving the robustness for shock, which is particularly important for space environments with larger shock accelerations.

Author Contributions: Conceptualization, G.X. and D.J.; methodology, G.X.; software, D.J.; validation, G.X. and D.J.; investigation, G.X.; data curation, L.Z. and J.L.; writing—original draft preparation, G.X.; writing—review and editing, G.X.; visualization, L.C. and L.Z.; supervision, R.D.; project administration, T.L. and J.W. All authors have read and agreed to the published version of the manuscript.

Funding: The project is partially supported by the Youth Innovation Promotion Association of the Chinese Academy of Sciences (Grant No. 1188000XGJ), the Chinese National Natural Science Foundation (Grant No. 11903041), and the Young Innovative Talents of the National Time Service Center of the Chinese Academy of Sciences (Grant No. Y917SC1).

Acknowledgments: We would like to acknowledge contributions of the strength check theory of the ultra-stable optical cavity to this paper from X. Zhang of Northwestern Polytechnical University, and F. Sun of National Time Service Center.

Conflicts of Interest: The authors declare no conflict of interest.

References

1. Katori, H. Optical lattice clocks and quantum metrology. *Nat. Photonics* **2011**, *5*, 203–210. [[CrossRef](#)]
2. Swallows, M.D.; Bishof, M.; Lin, Y.; Blatt, S.; Martin, M.J.; Rey, A.M.; Ye, J. Suppression of Collisional Shifts in a Strongly Interacting Lattice Clock. *Science* **2011**, *331*, 1043–1046. [[CrossRef](#)] [[PubMed](#)]

3. Huntemann, N.; Okhapkin, M.; Lipphardt, B.; Weyers, S.; Tamm, C.; Peik, E. High-Accuracy Optical Clock Based on the Octupole Transition in Yb⁺171. *Phys. Rev. Lett.* **2012**, *108*, 090801. [[CrossRef](#)]
4. Sherman, J.A.; Lemke, N.D.; Hinkley, N.; Pizzocaro, M.; Fox, R.W.; Ludlow, A.D.; Oates, C.W. High-Accuracy Measurement of Atomic Polarizability in an Optical Lattice Clock. *Phys. Rev. Lett.* **2012**, *108*, 153002. [[CrossRef](#)] [[PubMed](#)]
5. McFerran, J.J.; Yi, L.; Mejri, S.; Di Manno, S.; Zhang, W.; Guéna, J.; Le Coq, Y.; Bize, S. Neutral Atom Frequency Reference in the Deep Ultraviolet with Fractional Uncertainty = 5.7×10^{-15} . *Phys. Rev. Lett.* **2012**, *108*, 183004. [[CrossRef](#)] [[PubMed](#)]
6. Herrmann, S.; Senger, A.; Möhle, K.; Nagel, M.; Kovalchuk, E.V.; Peters, A. Rotating optical cavity experiment testing Lorentz invariance at the 10–17 level. *Phys. Rev. D* **2009**, *80*, 105011. [[CrossRef](#)]
7. Kennedy, C.J.; Oelker, E.; Robinson, J.M.; Bothwell, T.; Kedar, D.; Milner, W.R.; Marti, G.E.; Derevianko, A.; Ye, J. Precision Metrology Meets Cosmology: Improved Constraints on Ultralight Dark Matter from Atom-Cavity Frequency Comparisons. *Phys. Rev. Lett.* **2020**, *125*, 201302. [[CrossRef](#)]
8. Chou, C.W.; Hume, D.B.; Rosenband, T.; Wineland, D.J. Optical Clocks and Relativity. *Science* **2010**, *329*, 1630–1633. [[CrossRef](#)]
9. Jiang, H.; Kéfélian, F.; Crane, S.; Lopez, O.; Lours, M.; Millo, J.; Holleville, D.; Lemonde, P.; Chardonnet, C.; AmyKlein, A.; et al. Long-distance frequency transfer over an urban fiber link using optical phase stabilization. *J. Opt. Soc. Am. B* **2008**, *25*, 2029–2035. [[CrossRef](#)]
10. Predehl, K.; Grosche, G.; Raupach, S.M.F.; Droste, S.; Terra, O.; Alnis, J.; Legero, T.; Hansch, T.W.; Udem, T.; Holzwarth, R.; et al. A 920-Kilometer Optical Fiber Link for Frequency Metrology at the 19th Decimal Place. *Science* **2012**, *336*, 441–444. [[CrossRef](#)]
11. Barger, R.L.; Sorem, M.; Hall, J. Frequency stabilization of a cw dye laser. *Appl. Phys. Lett.* **1973**, *22*, 573–575. [[CrossRef](#)]
12. Drever, R.W.P.; Hall, J.L.; Kowalski, F.V.; Hough, J.; Ford, G.M.; Munley, A.J.; Ward, H. Laser phase and frequency stabilization using an optical resonator. *Appl. Phys. B* **1983**, *22*, 97–105. [[CrossRef](#)]
13. Millo, J.; Magalhães, D.; Mandache, C.; Le Coq, Y.; English, E.M.L.; Westergaard, P.G.; Lodewyck, J.; Bize, S.; Lemonde, P.; Santarelli, G. Ultrastable lasers based on vibration insensitive cavities. *Phys. Rev. A* **2009**, *79*, 053829. [[CrossRef](#)]
14. Chen, L.; Hall, J.; Ye, J.; Yang, T.; Zang, E.; Li, T. Vibration-induced elastic deformation of Fabry-Perot cavities. *Phys. Rev. A* **2006**, *74*, 053801. [[CrossRef](#)]
15. Leibrandt, D.R.; Thorpe, M.J.; Notcutt, M.; Drullinger, R.E.; Rosenband, T.; Bergquist, J.C. Spherical reference cavities for frequency stabilization of lasers in non-laboratory environments. *Opt. Express* **2011**, *19*, 3471–3482. [[CrossRef](#)] [[PubMed](#)]
16. Leibrandt, D.R.; Thorpe, M.J.; Bergquist, J.C.; Rosenband, T. Field-test of a robust, portable, frequency-stable laser. *Opt. Express* **2011**, *19*, 10278–10286. [[CrossRef](#)]
17. Vogt, S.; Lisdat, C.; Legero, T.; Sterr, U.; Ernsting, I.; Nevsky, A.; Schiller, S. Demonstration of a transportable 1 Hz-linewidth laser. *Appl. Phys. A* **2011**, *104*, 741–745. [[CrossRef](#)]
18. Webster, S.; Gill, P. Force-insensitive optical cavity. *Opt. Lett.* **2011**, *36*, 3572–3574. [[CrossRef](#)] [[PubMed](#)]
19. Argence, B.; Argence, B.; Prevost, E.; Lévêque, T.; le Goff, R.; Bize, S.; Lemonde, P.; Santarelli, G. Prototype of an ultra-stable optical cavity for space applications. *Opt. Express* **2012**, *20*, 25409–25420. [[CrossRef](#)]
20. Leibrandt, D.R.; Bergquist, J.C.; Rosenband, T. Cavity-stabilized laser with acceleration sensitivity below 10^{-12} g^{-1} . *Phys. Rev. A* **2013**, *87*, 023829. [[CrossRef](#)]
21. Chen, Q.; Nevsky, A.; Cardace, M.; Schiller, S.; Legero, T.; Häfner, S.; Uhde, A.; Sterr, U. A compact, robust, and transportable ultra-stable laser with a fractional frequency instability of 1×10^{-15} . *Rev. Sci. Instrum.* **2014**, *85*, 113107. [[CrossRef](#)] [[PubMed](#)]
22. Świerad, D.; Häfner, S.; Vogt, S.; Venon, B.; Holleville, D.; Bize, S.; Kulosa, A.; Bode, S.; Singh, Y.; Bongs, K.; et al. Ultra-stable clock laser system development towards space applications. *Sci. Rep.* **2016**, *6*, srep33973. [[CrossRef](#)]
23. Koller, S.B.; Grotti, J.; Vogt, S.; Al-Masoudi, A.; Dörscher, S.; Häfner, S.; Sterr, U.; Lisdat, C. Transportable Optical Lattice Clock With 7×10^{-17} Uncertainty. *Phys. Rev. Lett.* **2017**, *187*, 073601. [[CrossRef](#)]
24. Cao, J.; Zhang, P.; Shang, J.; Cui, K.; Yuan, J.; Chao, S.; Wang, S.; Shu, H.; Huang, X. A compact, transportable single-ion optical clock with 7.8×10^{-17} systematic uncertainty. *Appl. Phys. A* **2017**, *123*, 112. [[CrossRef](#)]
25. SOC2-Towards Neutral-Atom Space Optical Clocks. Available online: http://www.exphy.uni-duesseldorf.de/optical_clock/soc2/index.php (accessed on December 2011).
26. LISA-Laser Interferometer Space Antenna-NASA Home Page. Available online: <https://lisa.nasa.gov/index.html> (accessed on December 2017).
27. Luo, J.; Chen, L.-S.; Duan, H.-Z.; Gong, Y.; Hu, S.; Ji, J.; Liu, Q.; Mei, J.; Milyukov, V.; Sazhin, M.; et al. TianQin: A space-borne gravitational wave detector. *Class. Quantum Gravity* **2016**, *33*, 035010. [[CrossRef](#)]
28. Tao, B.; Chen, Q. A vibration-sensitive-cavity design holds impact of higher than 100 g. *Appl. Phys. B* **2018**, *124*, 228. [[CrossRef](#)]
29. Zhang, S. *Precise Generation and Transfer of Time and Frequency in NTSC*; ESA Topical Team on Geodesy and Clocks in Space: Munich, Germany, October 2018.
30. Hafiz, M.A.; Ablewski, P.; Masoudi, A.A.; Martínez, H.Á.; Balling, P.; Barwood, G.; Benkler, E.; Bober, M.; Borkowski, M.; Bowden, W.; et al. Guidelines for developing optical clocks with 10^{-18} fractional frequency uncertainty. *arXiv* **2019**, arXiv:1906.11495.
31. Chen, X.; Jiang, Y.; Li, B.; Yu, H.; Jiang, H.; Wang, T.; Yao, Y.; Ma, L. Laser frequency instability of 6×10^{-16} using 10-cm-long cavities on a cubic spacer. *Chin. Opt. Lett.* **2020**, *18*, 030201. [[CrossRef](#)]
32. Wang, S.; Cao, J.; Yuan, J.; Liu, D.; Shu, H.; Huang, X. Integrated multiple wavelength stabilization on a multi-channel cavity for a transportable optical clock. *Opt. Express* **2020**, *28*, 11852. [[CrossRef](#)] [[PubMed](#)]

33. Nitiss, E.; Bluss, K.; Alnis, J. Numerical 2D and 3D simulations of a spherical Fabry-Perot resonator for application as a reference cavity for laser frequency stabilization. *Latv. J. Phys. Tech. Sci.* **2015**, *52*, 21–33. [[CrossRef](#)]
34. Tai, Z.; Yan, L.; Zhang, Y.; Zhang, X.; Guo, W.; Zhang, S. Transportable 1555-nm ultra-stable laser with sub-0.185-Hz linewidth. *Latv. J. Chin. Phys. Lett.* **2017**, *34*, 090602. [[CrossRef](#)]
35. Häfner, S.; Herbers, S.; Vogt, S.; Lisdat, C.; Sterr, U. Transportable interrogation laser system with an instability of mod $\sigma_y = 3 \times 10^{-16}$. *Opt. Express* **2020**, *28*, 16407–16416. [[CrossRef](#)] [[PubMed](#)]
36. Parker, B.; Marra, G.; Johnson, L.; Margolis, H.; Webster, S.; Wright, L.; Lea, S.; Gill, P.; Bayvel, P. Transportable cavity-stabilized laser system for optical carrier frequency transmission experiments. *Appl. Opt.* **2014**, *53*, 8157–8166. [[CrossRef](#)] [[PubMed](#)]
37. *Space Station Application System Payload Environmental Test Requirements, China*; Department of Space Science and Applications, Chinese Academy of Sciences: Beijing, China, 2014.
38. GJB150. 1A-2009, Laboratory Environmental Test Methods of Military Materiel. Available online: <https://www.renrendoc.com/p-881076.html> (accessed on December 2009).
39. Hayashi, K.; Easier, T.; Bradt, R. A Fracture Statistics Estimate of a Borosilicate Glass of the Fatigue Limit of a Borosilicate Glass. *J. Eur. Ceram. Soc.* **1993**, *12*, 487–491. [[CrossRef](#)]
40. Zilcha, O.; Quinn, G.D.; Rowe, J.M.; Pierce, D.J. Investigation into the Mechanical Cause of Failure of Neutron Guide NG-2 at the NIST Research Reactor. *J. Fail. Anal. Prev.* **2012**, *12*, 604–616. [[CrossRef](#)]
41. SCHOTT Technical Information No. 33: “Design Strength of Optical Glass and ZERODUR®”. Available online: http://www.us.schott.com/advanced_optics/english/tools_downloads/download/index.html#Technical%20Information (accessed on December 2004).
42. Wickert, J. *An Introduction to Mechanical Engineering*, 1st ed.; Cengage Learning: Boston, MA, USA, 2004; p. 157.